Design of SIW Cavity-Backed Circular-Polarized Antennas Using Two Different Feeding Transitions

Dong-Yeon Kim, Jae W. Lee, Taek K. Lee, and Choon Sik Cho

***Abstract*—Two circular-polarized circular patch antennas which have novel feeding structures such as a substrate integrated waveguide (SIW), a cavity-backed resonator and two different feeding transitions, are proposed and experimentally investigated in terms of electrical performances, including reflection coefficients, optimized parameter values, circular polarized antenna gain, axial ratios and radiation patterns. By inserting asymmetrical inductive via arrays into the interface region between the circular patch and SIW feeding structure, it is found that an enhancement of input impedance bandwidth has been achieved. In addition, in order to check the effects of feeding transition types on the electrical performances of the main radiator, two different feeding transitions, namely microstrip-to-SIW and coax-to-SIW, have been studied by considering reflection coefficients, gain, axial ratios and radiation patterns. As a result, it is experimentally proved that a broadband impedance bandwidth of 17.32% and 14.42% under the criteria of less than VSWR 2:1 and 1.5:1, respectively, have been obtained and an RHCP axial ratio of 2.34% with a maximum gain of 7.79 dBic has been accomplished by using the proposed antenna with coax-to-SIW transition operating at the X-band of 10 GHz center frequency.**

***Index Terms*—Asymmetric inductive diaphragm, cavity-backed resonator, circular polarization, sequential feeding, substrate integrated waveguide (SIW).**

I. Introduction

Until now, a variety of satellite antennas have been designed and suggested because of their importance in satellite communication. The general requirements for satellite antennas are light weight, stabilized gain, good return loss characteristics and a compatible radiation pattern to narrow/wideband electromagnetic interferences caused by unexpected aerospace environmental phenomena. First and foremost, circularly polarized characteristics in antennas are the most important in many wireless communication systems, including in satellite communication. In order to generate circular polarization (CP) in an antenna, a perturbed circular patch and microstrip [1], [2]/aperture coupled feeding [3] has been conventionally used at the expense of transmission line loss.

Moreover, array antennas employing sequentially rotated feeding networks have been implemented to improve total antenna gain, the purity of axial ratio and axial ratio bandwidth [4]. In [5] considering the structure of 2×16 phased array antennas suitable for the generation of circular polarization at Ku-band, it is conjectured that the axial ratio and feeding losses of each element have been improved by applying the notch and stub and using a hollow metallic rectangular waveguide, respectively. However, as a drawback, the structure proposed in [5] is a little bulky. Hence, in order to complement this shortcoming in terms of the bulky feeding structure, a feeding network adopting partially substrate integrated waveguide (SIW) technology has been introduced to replace the conventional metallic waveguide [6]. Nevertheless, the microstrip line, which may lead to distortion and degradation in radiation characteristics, still exists for sequentially rotated feeding. Consequently, single or array antennas fed by well-established SIW transmission lines or sequentially rotated feeding networks are required to minimize the distortion of radiation characteristics. In general, SIW is well known as a representative transmission line with low loss replacing the conventional microstrip line which causes performance degradation due to the co-existence in the same plane with the antenna radiator in terms of reflection coefficient and axial ratio. In addition, it has some advantages in terms of its high power signal transfer and miniaturization with the help of the rectangular waveguide type and easy fabrication on PCB, respectively [7].

As a good candidate for low loss antennas, various types of LP- and CP-generating antennas using SIW technology have been developed and studied [8], [9] and [12]. The authors in [8], [9] have suggested an X-band LP-generating planar slot antenna and RHCP antenna generating two orthogonal cavity modes as a function of lengths of two crossed slot arms. Even though the previously suggested structures in [8], [9] have adopted GCPW feeding networks and obtained good electrical performances, they have had some drawbacks such as a narrow impedance bandwidth of less than 3%.

On the other hand, the authors of this work have already published work regarding a CP-generating antenna using an SIW-based circular ring-slot as a single element [12]. In the proposed structure in [12], the RHCP generation has been obtained as a result from the separation of the single resonant mode to dual resonant modes with two orthogonal zero-potential planes having a phase difference of 90°. At the same time, a wide impedance bandwidth of 18.74% (VSWR 2:1) has been achieved through the use of an asymmetric inductive diaphragm embedded into the SIW feeding part.

As another method for increasing the impedance bandwidth, reflection-canceling posts and slots have been introduced in [10], [11].

In this communication, an RHCP-generating SIW single antenna suitable for an element of sequentially rotated phased array antennas is proposed for high data transfer rate in satellite communication. Particularly, the proposed SIW antenna with a cavity-backed resonator is unified into the SIW feeding network with two different transitions by differentiating from the conventional single antenna using a microstrip feeding line.

II. Proposed Antenna Geometry and Design Procedures

On the contrary to a single antenna element employing a conventional microstrip feeding line, an SIW-fed structure, which leads to an enhancement of the shielding effect protecting from the external noise and induces a stabilization of radiation patterns, is proposed by using metallic via arrays acting as a perfect electric wall (PEW). The proposed antenna geometry shown in Fig. 1 is mainly composed of three parts. The first one is a combination of a conventional perturbed circular patch with a shorted-end via (or probe) and an SIW cavity where the former is essential for the generation of circular polarization and the latter is for a higher gain and a lower backlobe radiation. The second one is an SIW-fed impedance matching network integrated with an asymmetric inductive diaphragm using via arrays. The role of this impedance matching network has been already clarified in [12]. The last one is a microstrip-to-SIW transition in Fig. 1(a) or coax-to-SIW transition in Fig. 1(b) essential for measurements. The total occupying

Manuscript received November 03, 2009; revised June 13, 2010; accepted September 14, 2010. Date of publication January 31, 2011; date of current version April 06, 2011. This work was supported by the NSL (National Space Lab) program through the Korea Science and Engineering Foundation funded by the Ministry of Education, Science and Technology (no. S10801000159-08A0100-15910).

D.-Y. Kim is with the Institute of New Media Communication, School of Electrical Engineering and Computer Science, Seoul National University, Seoul 151-742, Korea (e-mail: dykim@ael.snu.ac.kr).

J. W. Lee, T. K. Lee and C. S. Cho are with the School of Electronics, Telecommunication and Computer Engineering, Korea Aerospace University, Goyang, Gyeonggi-do, Korea (e-mail: jwlee1@kau.ac.kr; tklee@kau.ac.kr; cscho@kau.ac.kr).

Color versions of one or more of the figures in this communication are available online at http://ieeexplore.ieee.org.

Digital Object Identifier 10.1109/TAP.2011.2109675

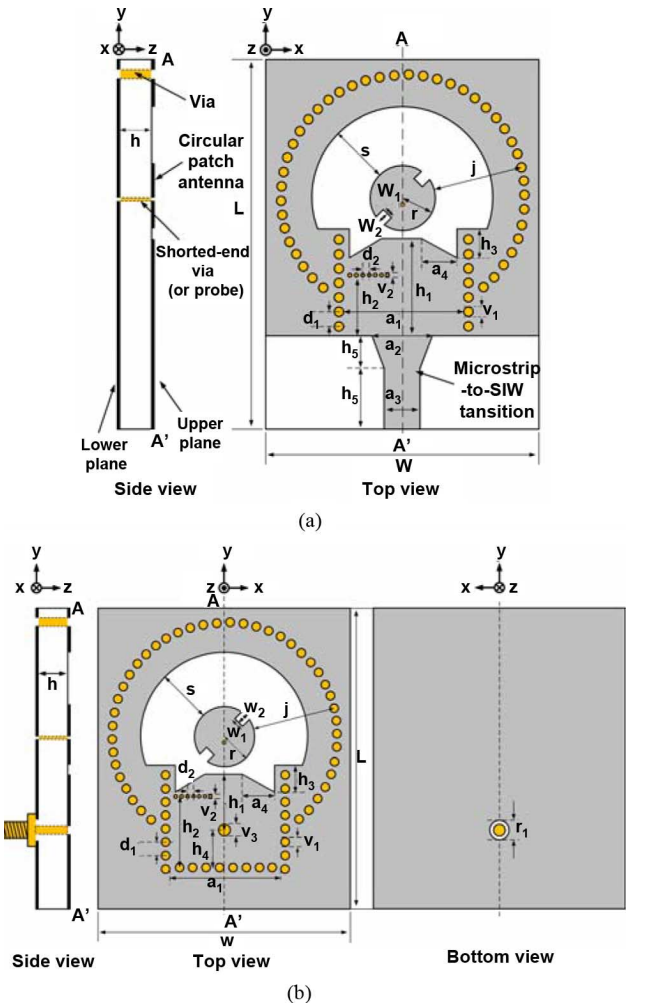

Fig. 1. Proposed antenna geometry using (a) microstrip-to-SIW transition and (b) coax-to-SIW transition.

TABLE I
PROPOSED ANTENNA PARAMETERS AND OPTIMIZED VALUES ACCORDING TO THE TRANSITION TYPES

Parameters	Values (mm)		Parameters	Values (mm)
	μ-strip	coax		
a_1	16		h_6	5
a_2	8		j	10.55
a_3	4.9		L	45.2
a_4	4.5		r	4.65
d_1	1.5		r_1	3.2
d_2	0.7		s	7
h	1.57		v_1	1
h_1	9.6	4.36	v_2	0.3
h_2	6.72	6.78	v_3	1.3
h_3	3.292	4.64	W	35
h_4	3.2		w_1	1.92
h_5	10		w_2	1.315

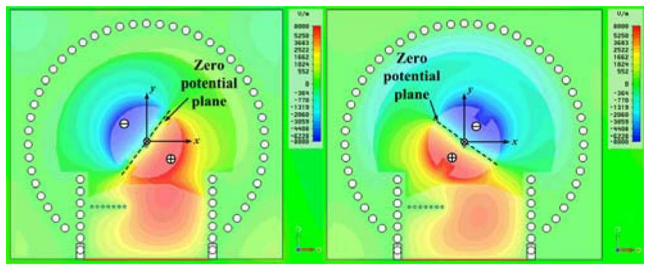

Fig. 2. Electric field distributions inside the cavity at each resonant frequency (a) the first resonant TM11-mode at 9.89 GHz and (b) the second resonant TM11-mode at 10.58 GHz.

area including transition region is $35\ \mathrm{mm} \times 45.2\ \mathrm{mm}$. The entire antenna structure has been designed by employing an RT/Duroid 5880 substrate as a single layer having a relative permittivity of 2.2, loss tangent of 0.0009 at 10 GHz and a thickness of 1.57 mm. The final optimized parameter values according to the transition types are listed in Table I.

A. Radiating Element for Generating Circular Polarization

The used circular patch operating at 10 GHz with the RHCP characteristic is proposed and designed by using a conventional equation [13], resulting in 5.2 mm as a radius (r). The roughly estimated initial value of the main radius has been optimized to 4.65 mm with the help of commercially available software, CST MWS based on a finite-difference time-domain algorithm [14]. The finally optimized value includes the coupling effects between the upper metal plate of the SIW feeding structure and the circular patch mounted on the upper patch.

From the reflection characteristics of the CP-generating circular patch proposed in this communication, it seems that the dual resonance is due to the separation into the dual resonant TM_{11}-mode at the nearest resonant frequencies of the single resonant TM_{11}-mode generated by the conventional perturbed ratio $(\Delta s/S)$ of the circular patch. This phenomenon can be explained through the electric field distributions inside the cavity as shown in Fig. 2. As a detailed description, at first, Fig. 2(a) depicts the electric field distributions at 9.89 GHz as a lower resonant frequency and shows the zero-potential plane formed at azimuthal angles (ϕ) of 45° and 225°. On the other hand, it is conjectured that the upper resonant frequency occurs at 10.58 GHz as shown in Fig. 2(b) due to the reduced size. At this time, the zero-potential plane is located at 135° and 315° in an azimuthal angle. Hence, the two zero-potential planes are orthogonal and form a phase difference of 90° each other. This phase difference leads to an RHCP rotation of the electric field inside the cavity and a maximum purity of axial ratio around 10 GHz as a center frequency.

The perturbed design parameters, w_1 and w_2, determining the generation of dual TM_{11}-modes occupy the total area $\Delta s = 2\,(w_1 \cdot w_2) = 2(w_1)^2/x = 2x \cdot (w_2)^2$ and govern the ratio of the perturbed and original circular patch area $(k = \Delta s/S)$. The parameter indexes x and k defined as $x = w_1/w_2$ and $k = \Delta s/S$ are essential for accomplishing the electrical performances such as the lower reflection coefficients, an enhancement of the optimized axial ratio bandwidth and purity improvement and could be optimized to 1.357 when $w_1 = 1.92\ \mathrm{mm}$ and $w_2 = 1.415\ \mathrm{mm}$ and 0.08, respectively.

As another critical parameter for generating RHCP, a shorted-end via connected between the circular patch on the upper plate and ground plane on the lower plate is located at a position 0.5 mm away from the center of the circular patch to the negative y direction with a via diameter of 0.3 mm such that zero-reference planes indicating zero-field points in a SIW cavity constitutes 90° in a rotational angle. In addition, the circular array vias (j) replacing a metalized circular-cylindrical

cavity has been adopted for performance improvement in radiation patterns and gain. Finally, the distance, s, between the circular patch and the upper metal plate of SIW cavity has been controlled for obtaining the minimum effect on the self-resonance of the circular patch and optimized by an EM full-wave simulator.

B. SIW Feeding Structure With Embedded Impedance Matching Circuitry

The width, a_1, of the SIW feeding structure within the operating frequency regime from 8.2 to 12.4 GHz has been determined as 16 mm by setting the cutoff frequency of the fundamental mode (TE_{10}-mode) to approximately 6.3 GHz. Moreover, in order to minimize the leakage property, including radiation loss through side walls, conduction loss and dielectric loss due to the imperfect manufacturing process of metalized via arrays, the diameter (v_1) of vias and the distance (d_1) between vias have been optimized to 1 mm and 1.5 mm, respectively, by considering the conditions of $d_1/v_1 < 2.5$ and $v_1/a_1 < 1.8$ [15].

Consider the antenna configuration with the traveling wave-type SIW feeding structure as shown in Fig. 1. The important parameters for this configuration are the pattern parameters, a_4 and h_3, etched on the upper plane and the distance, h_1, of the SIW feeding line from each transition. Especially, since the fundamental TE_{10}-mode of SIW and the resonant TM_{11}-mode of the perturbed circular patch are different from each other, the optimized parameters considering the smooth energy transition are required to satisfy the matched impedance characteristics.

Figs. 3(a) and 3(c) show the reflection coefficients or impedance matching characteristics according to the variations of h_1 and h_3, respectively. As a result, it is obtained that the optimized parameters of the proposed antenna using microstrip-to-SIW transition h_1 and h_3 are 9.6 mm and 3.292 mm, respectively, for achieving the maximum impedance bandwidth under the condition of less than VSWR 1.5:1 and an improvement of more than 10 dB with respect to the reflection coefficients.

As a function of additional impedance matching to overcome the narrow bandwidth characteristic due to the microstrip patch antenna, metallic via arrays with parameters d_2 and v_2 acting as an asymmetric inductive diaphragm with zero thickness have been introduced, inserted and unified into the SIW feeding structure. Fig. 3(b) shows the impedance matching characteristics according to the parameter h_2 which is the distance between the asymmetrical inductive via arrays and the feeding line as shown in Fig. 1(a). In a similar way, the parameter h_2 in the case of coax-to-SIW transition as shown in Fig. 1(b), showing the distance between asymmetrical inductive via arrays and the back-shorted via arrays, can be optimized.

The asymmetric inductive diaphragm in Fig. 4(b) can be modeled by a shunt inductor in a two-port network and the magnitude of susceptance (Z_0/X) is controlled by the width of the diaphragm (d' in Fig. 4(a)) [16]. In addition, the width of the diaphragm is dependent on the number of via arrays and the separate distance (d_2). Here, Z_0 means the wave impedance of the rectangular waveguide. As shown in Fig. 3(d) and (e), the matching condition at the antenna input port can be obtained from the variation of the width of the SIW-based asymmetric inductive diaphragm. In practical situations, to realize the via arrays with radii as small as possible to take into account the theoretical via effect of zero thickness as suggested in [16], v_2, the diameter of via has been set up to be 0.3 mm.

On the other hand, Fig. 5 delineates the input impedance variation at the feeding point according to the number of via arrays. From the impedance loci within the frequency range (8.79 to 10.84 GHz), it is seen that the inductive characteristic is dominant and the loci move to the center point. As an optimized via array, a case of 7 EA vias shown in Fig. 5 has been selected and makes the input impedance locus entirely move to the inside of a circle satisfying $\mathrm{VSWR} = 2$. The physical behavior means that the total width of via arrays plays a role in the

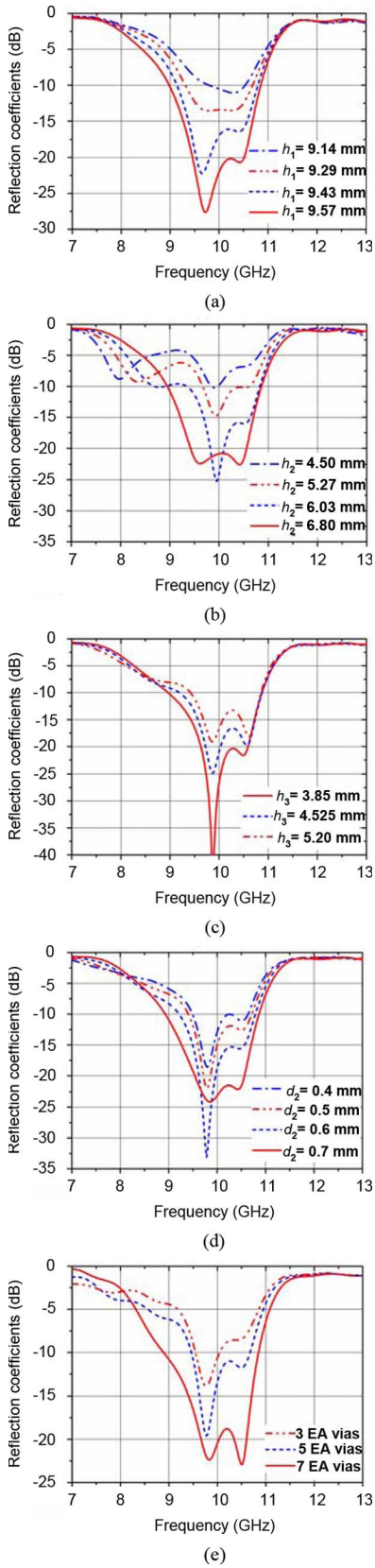

Fig. 3. Impedance matching characteristics according to the variation of (a) h_1, (b) h_2, (c) h_3, (d) d_2, (e) the number of via arrays consisting of asymmetric inductive diaphragm in Fig. 1 (the other parameter values are fixed as in Table I).

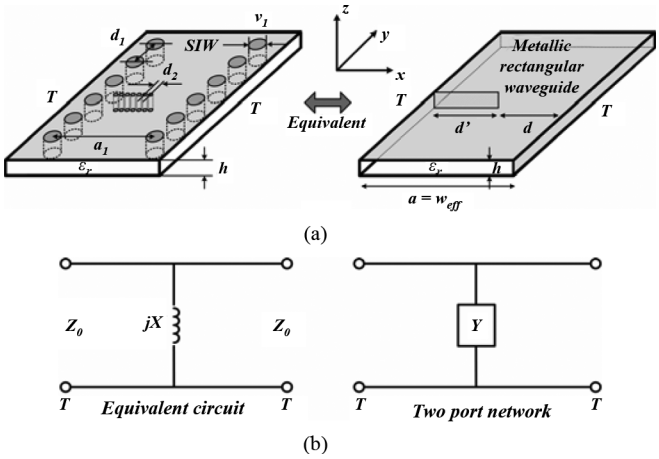

Fig. 4. Embedded asymmetric inductive diaphragm (a) SIW impedance matching circuitry and its equivalent metallic rectangular waveguide model. (b) Equivalent circuit.

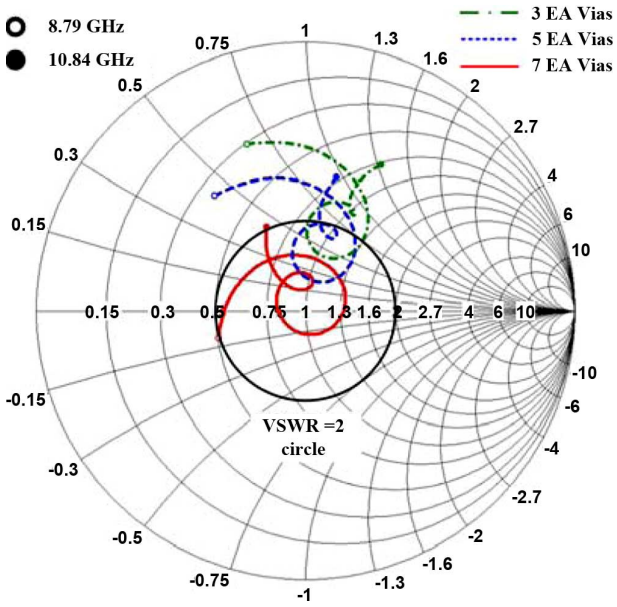

Fig. 5. Input impedance variation of proposed antenna according to the number of asymmetric inductive diaphragm via.

generation of additional susceptance to the equivalent input circuit and making the imaginary part of input impedance zero. As a result, it is ensured that the optimum solution for input impedance matching could be obtained from the variations of the number of via arrays and the control of distance between the nearest vias as shown in Figs. 3(d) and 3(e). Furthermore, the optimum position of SIW-based matching circuitry comprising via array is mainly dependent on the design parameter h_2 as shown in Fig. 1 and has been determined from the parametric studies using an FDTD-based commercially available simulator. At this time, the simulated results in Fig. 3 have been computed according to the variation of interested parameters in each plot by fixing the other parameters as the same as the values listed in Table I.

C. Two Types of Transition for Measurements

In order to extract the electrical characteristics of only the proposed antenna, it is necessary to design the transition having a lower return loss and higher transfer characteristics without the distortion in radiation properties. Two types of transitions, microstrip-to-SIW and

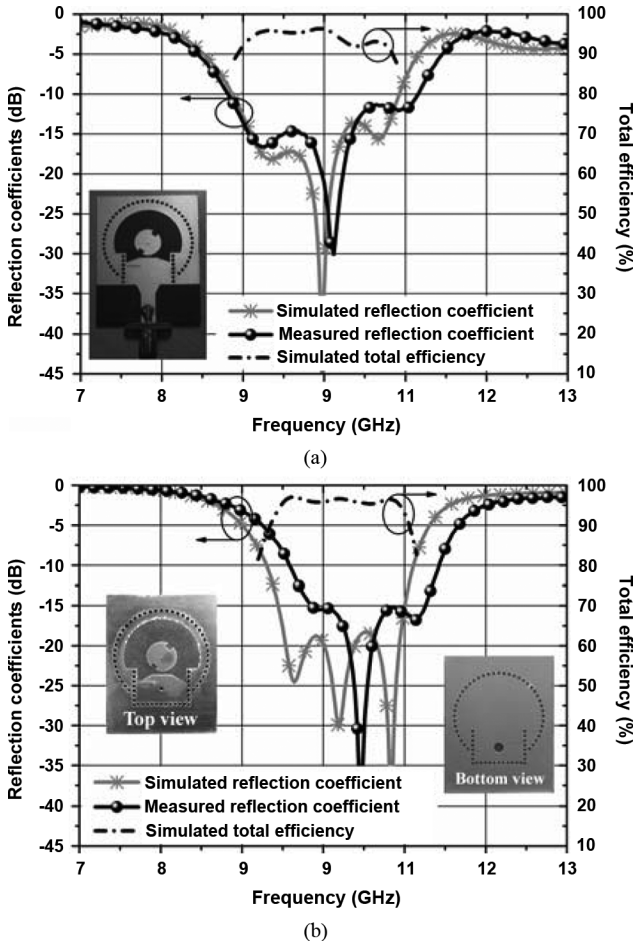

Fig. 6. The reflection coefficients and simulated total efficiency of two proposed antennas using (a) microstrip-to-SIW transition and (b) coax-to-SIW transition, respectively.

coax-to-SIW, have been proposed and implemented for measurement [17], [18]. In the case of microstrip-to-SIW transition transforming quasi TEM-mode into SIW fundamental TE_{10}-mode as shown in Fig. 1(a), the antenna parameters of a_2 and h_4 for transition have been optimized for the proper transfer characteristics and summarized in Table I. On the other hand, in order to obtain the optimized impedance matching and an enhancement of impedance bandwidth, the capacitive ring slot shown in Fig. 1(b) has been inserted into a lower conductor plate of the PCB substrate with diameter r_1, equal to 3.2 mm in the case of coax-to-SIW transition [18]. As a critical element for easy power transition, the feeding point h_6 of the SMA connector shown in Fig. 1(b) should be located at $\lambda_g/4$ away from the back-shorting via arrays preventing the reflected power from being cancelled, where λ_g means the guided wavelength.

III. Results and Discussion

The reflection coefficients of the proposed antennas with two different feeding structures have been simulated and measured by using an EM full-wave simulator and Agilent vector network analyzer (N5230A) in a laboratory environment. Fig. 6 shows a good agreement between the simulated and measured data in both of the cases using the two different feeding structures. In addition, the simulated total efficiency is suggested in Fig. 6 with the measured reflection coefficients. In both cases, the total radiating efficiency is more than 90% by taking the finite conductivity of the copper and the loss tangent of the considered dielectric material during the simulation process.

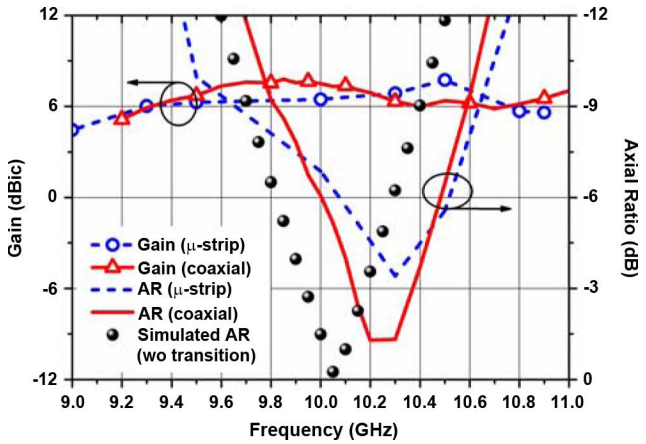

Fig. 7. Measured right-handed circular polarized (RHCP) gain and axial ratio results of two proposed antennas, respectively.

In the case of using microstrip-to-SIW transition, as in Fig. 1(a), it is seen from Fig. 6(a) that the simulated impedance bandwidths are 2.06 GHz ranging from 8.87 to 10.93 GHz and 1.25 GHz raging from 9.06 to 10.31 GHz, respectively, under the criteria of VSWR 2:1 and 1.5:1, whereas the measured results are 2.33 GHz (from 8.82 to 11.15 GHz) and 1.36 GHz (from 9.02 to 10.38 GHz), respectively, under the conditions of less than VSWR 2:1 and 1.5:1. On the other hand, Fig. 6(b) shows that in the case of using coax-to-SIW transition, as in Fig. 1(b), the simulated (measured) impedance bandwidths are 1.815 GHz (1.82 GHz) and 1.6 GHz (1.52 GHz), respectively, under the same conditions listed above.

As additional aspects to antenna performances, the axial ratios of RHCP and gain characteristics have been treated in Fig. 7. As a reference in CP purity, the simulated data using only a waveguide port without transition, which is impractical in real situations and results in -3 dB axial ratio bandwidth ranging from 9.94 to 10.18 GHz, have been included for comparison in Fig. 7. As expected from Figs. 7 and 8, the maximum axial ratio of the SIW antenna using microstrip-to-SIW transition amounts to approximately -3.4 dB at 10.3 GHz and leads to the degradation of purity in RHCP generation. It is conjectured that one of the reasons is due to the generation of higher-order modes from the wide line width caused by employing the substrate of lower permittivity and relatively higher thickness. As another reasonable effect on CP purity, the co-existence of a soldered SMA connector on the input port and circular patch radiator positioned in the same direction on the upper plane may have a possibility of affecting the radiation pattern and axial ratio characteristics. As a result, the enhanced purity of axial ratio and stable high gain more than 6 dBic over the operating bandwidth with maximum RHCP gain, 7.79 dBic at 9.85 GHz, can be obtained by using coax-to-SIW transition as shown in Fig. 7. From Figs. 7 and 9, which show the measured axial ratio and radiation patterns, it is seen that the maximum axial ratio and -3 dB bandwidth in axial ratio of the proposed antenna using coax-to-SIW transition are -1.3 dB at 10.2 GHz and 240 MHz ranging from 10.13 to 10.37 GHz, respectively, which are almost similar to the simulated data. In addition, Figs. 8 and 9, which show the radiation patterns according to the transition types, represent that the proposed antenna employing coax-to-SIW transition has more stable RHCP radiation patterns and a lower level in cross-polarization than that using microstrip-to-SIW transition. However, as a disadvantage of the proposed antenna radiator without transition structure, it is noticed that the beam-tilting phenomenon in *yz* plane should occur because of the mismatch at the boundary between the SIW transmission line and probe in the circular patch.

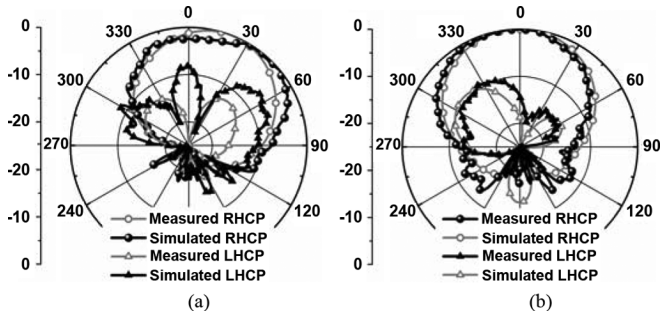

Fig. 8. Radiation patterns of the proposed antenna using microstrip-to-SIW transition at 10.3 GHz (a) *yz* plane (b) *zx* plane.

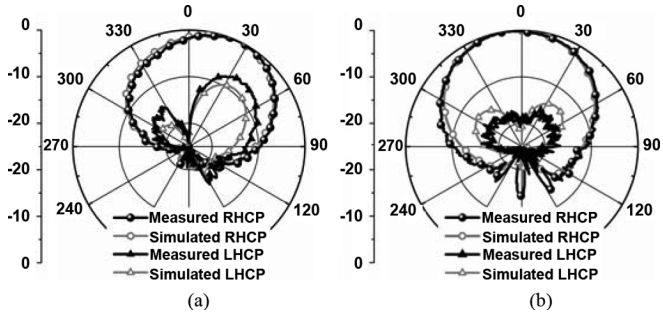

Fig. 9. Radiation patterns of the proposed antenna using coax-to-SIW transition at 10.2 GHz (a) *yz* plane and (b) *zx* plane.

IV. Conclusion

A circularly polarized antenna with a unified integration of matching feeding structure and SIW-typed cavity in a single layer has been suggested and implemented in this communication. Particularly it is shown that the low loss characteristic of the feeding line and broadband impedance bandwidth of the proposed antenna have been accomplished by using an SIW structure compared to the conventional microstrip transmission line. In addition, in order to improve the reflection coefficients remarkably, the asymmetric inductive diaphragm consisting of via arrays has been adopted as a control of input susceptance. In terms of input impedance bandwidth, it is found that the optimized antenna results in 17.32% and 14.42% as a percentage bandwidth under the criteria of less than VSWR 2:1 and 1.5:1, respectively. From the results of comparison of the radiation patterns in *yz*- and *zx*-plane, it is seen that the cross-polarization level of the coax-to-SIW transition case is lower than that of the microstrip-to-SIW transition case. Furthermore, it is guaranteed that the single element and the low-loss feeding network using SIW can be easily extended to array systems and low loss multi-port feeding networks in satellite communication.

References

[1] M. Haneishi, S. Yoshida, and N. Goto, "A broadband microstrip array composed of single-feed type circularly polarized microstrip antennas," in *Proc. IEEE Antennas and Propag. Symp.*, May 1982, vol. 20, pp. 160–163.

[2] W.-K. Lo, C.-H. Chan, and K.-M. Luk, "Bandwidth enhancement of circularly polarized microstrip patch antenna using multiple L-shaped probe feeds," *Microw. Opt. Technol. Lett.*, vol. 42, no. 4, pp. 263–265, Aug. 2004.

[3] A. Ghiotto, M. Bourry, and K. Wu, "Cross-slot coupled elliptical patch antenna circularly polarized for localization," *Microw. Opt. Technol. Lett.*, vol. 49, no. 2, pp. 336–339, Feb. 2007.

[4] P. S. Hall, "Application of sequential feeding to wide bandwidth, circularly polarized microstrip patch arrays," in *Inst. Elect. Eng. Proc. H*, Oct. 1989, vol. 136, pp. 390–398.
[5] M. Shahabadi, D. Busuioc, A. Borji, and S. Safavi-Naeini, "Low-cost, high-efficiency quasi-planar array of waveguide-fed circularly polarized microstrip antennas," *IEEE Trans. Antennas Propag.*, vol. 53, no. 6, pp. 2036–2043, Jun. 2005.
[6] A. Borji, D. Busuioc, and S. Safavi-Naeini, "Efficient, low-cost integrated waveguide-fed planar antenna array for Ku-band applications," *IEEE Antennas Wireless Propag. Lett.*, vol. 8, pp. 336–339, 2008.
[7] Y. J. Cheng, K. Wu, and W. Hong, "Power handling capability of substrate integrated waveguide interconnects and related transmission line systems," *IEEE Trans. Adv. Packag.*, vol. 31, pp. 900–909, Nov. 2008.
[8] G. Q. Luo, Z. F. Hu, L. X. Dong, and L. L. Sun, "Planar slot antenna backed by substrate integrated waveguide cavity," *IEEE Antennas Wireless Propag. Lett.*, vol. 7, pp. 236–239, 2008.
[9] G. Q. Luo, Z. F. Hu, Y. Liang, L. Y. Yu, and L. L. Sun, "Development of low profile cavity backed crossed slot antennas for planar integration," *IEEE Trans. Antennas Propag.*, vol. 57, no. 10, pp. 2972–2979, Oct. 2009.
[10] S. Park, Y. Okajima, J. Hirokawa, and M. Ando, "A slotted post-wall waveguide array with interdigital structure for 45° linear and dual polarization," *IEEE Antennas Propag.*, vol. 53, no. 9, pp. 2865–2871, Sep. 2005.
[11] J. Hirokawa and M. Ando, "45° linearly polarized post-wall waveguide- fed parallel-plate slot arrays," *Proc. Inst. Elect. Eng. Microw. Antennas Propag.*, vol. 147, pp. 515–519, Dec. 2000.
[12] D. Kim, J. W. Lee, C. S. Cho, and T. K. Lee, "X-band circular ring-slot antenna embedded in single-layered SIW for circular polarization," *Electron. Lett.*, vol. 45, no. 13, pp. 668–669, Jun. 2009.
[13] C. A. Balanis, *Antenna Theory: Analysis and Design*. Hoboken, NJ: Wiley, 2005, ch. 14.
[14] CST Microwave Studio (MWS) CST Corporation, 2008 [Online]. Available: http://www.cst.com
[15] M. Bozzi, M. Pasian, L. Perregrini, and K. Wu, "On the losses in substrate integrated waveguides," in *Proc. 37th Eur. Microwave Conf.*, Munich, Germany, Oct. 2007, pp. 384–387.
[16] N. Marcuvitz, *Waveguide Handbook*. New York: McGraw-Hill, 1951.
[17] D. Deslandes and K. Wu, "Integrated microstrip and rectangular waveguide in planar form," *IEEE Microwave Wireless Compon. Lett.*, vol. 11, no. 2, pp. 68–70, Feb. 2001.
[18] K. Song, Y. Fan, and Y. Zhang, "Eight-way substrate integrated waveguide power divider with low insertion loss," *IEEE Trans. Microwave Theory Tech.*, vol. 56, pp. 1473–1477, Jun. 2008.

UWB Dielectric Resonator Antenna Having Consistent Omnidirectional Pattern and Low Cross-Polarization Characteristics

Kenny Seungwoo Ryu and Ahmed A. Kishk

***Abstract*—A new simple compact monopole type dielectric resonator antenna (DRA) for ultrawideband (UWB, 3.1-10.6 GHz) applications is presented. The design combines the advantages of small size DRA and thin planar monopole antennas. The design provides high-radiation efficiency, consistent omnidirectional characteristics, and low cross polarization within the entire band. The antenna size is 15×33 mm^2 with 5.08 mm thickness. The dielectric resonator (DR) is shaped to house the excitation feed and the dielectric substrate is cut to house the DR. The coplanar waveguide is used to feed the antenna.**

***Index Terms*—Dielectric resonator (DR) antenna, low cross-polarization level, omnidirectional pattern, ultrawideband (UWB) antenna.**

I. Introduction

Recently, many UWB antennas have been proposed [1]–[6], since the Federal Communication Commission (FCC) allowed 3.1–10.6 GHz unlicensed band for UWB communication.

Challenges of the feasible UWB antenna design include the UWB performance issues of the sufficient impedance matching bandwidth, the compact antenna size, high radiation efficiency, avoiding the interference problem of the nearby communication band, constant gain, constant group delay or linear phase, and getting a consistent uniform radiation pattern to avoid undesirable distortions of the radiated and received pulse [1]. Lots of efforts have been performed to improve the performance of the UWB antenna especially to avoid the interference problem [2]–[4]. However, among them, the radiation pattern problems of the UWB antenna still need to be solved, because omnidirectional or near-omnidirectional radiation patterns (defined for [7] to be gain variations less than 3 dB in the H plane) usually cannot be achieved for higher operating frequencies. Some techniques such as the step shaped element [7], orthogonal element [8], and S-shaped element [9] for the broadband monopole antenna were proposed to improve the omnidirectional radiation pattern characteristics within the whole operating frequency band. In addition, planar broadband monopole antennas are known to suffer from high cross-polarization radiation levels [1]. However, no efforts were reported to reduce the cross-polarization levels with consistent omnidirectional patterns for the planar broadband monopole antennas.

The dielectric resonator antenna (DRA) is one of the attractive candidate antennas for UWB application due to several striking characteristics such as high radiation efficiency, low dissipation loss, light weight, and small size. Significant efforts for the DRA have been reported to achieve wide bandwidth enhancements over the past two decades [10]–[17].

Manuscript received October 13, 2009; revised August 16, 2010; accepted August 25, 2010. Date of publication January 31, 2011; date of current version April 06, 2011.

The authors are with the Department of Electrical Engineering, University of Mississippi, University, MI 38677 USA (e-mail: kennyryu77@yahoo.com).

Color versions of one or more of the figures in this communication are available online at http://ieeexplore.ieee.org.

Digital Object Identifier 10.1109/TAP.2011.2109676